

DR. EFTHIMIOS GAZELAKIS (Orcid ID : 0000-0002-3346-9281)

Article type : Novel Development

The Biomechanical Profile of an Osseo-integrated Rectangular Block Implant: A Pilot In Vivo Experimental Study.

Efthimios Gazelakis., Roy B. Judge., Joseph E. A. Palamara.

E. Gazelakis: Honorary Clinical Fellow, Melbourne Dental School, University of Melbourne.
egazelakis@unimelb.edu.au, +61 412246921

R.B. Judge: Head, Department of Prosthodontics, Melbourne Dental School, University of Melbourne.
roybj@unimelb.edu.au, +61 421059293

J.E.A. Palamara: Senior Lecturer, Restorative Dentistry, Melbourne Dental School, University of Melbourne.
palamara@unimelb.edu.au, (61) 03 93411532

Author's Contributions:

E. Gazelakis: Conceptualization-Lead, Data curation-Lead, Formal analysis-Lead, Funding acquisition-Lead, Investigation-Lead, Methodology-Lead, Project administration-Lead, Writing-original draft-Lead.

R.B. Judge: Conceptualization-Equal, Funding acquisition-Equal, Methodology-Equal, Project administration-Equal, Supervision-Lead, Writing-review & editing-Equal.

J.E.A. Palamara: Conceptualization-Equal, Data curation-Equal, Formal analysis-Equal, Investigation-Equal, Methodology-Equal, Supervision-Equal, Writing-original draft-Equal

Abstract:

Objective: A novel implant design, the Rectangular Block Implant (RBI), was investigated as a possible solution to the restoration of the posterior resorbed ridge.

This is the author manuscript accepted for publication and has undergone full peer review but has not been through the copyediting, typesetting, pagination and proofreading process, which may lead to differences between this version and the [Version of Record](#). Please cite this article as [doi: 10.1111/CLR.13834](https://doi.org/10.1111/CLR.13834)

This article is protected by copyright. All rights reserved

Aim: To maximally load test the osseointegrated RBI in shear and tensile loads and relate these findings to known human masticatory loads as biomechanical proof of the study concept.

Materials and methods: Twelve RBIs were design-manufactured and placed into posterior mandibular saddles in 3 mature greyhound dogs. - 2 per left and right.

After 12 weeks of healing, osseointegration was confirmed using resonance frequency analysis (RFA) and wrench torque tests. Three bone blocks each with two RBIs were dissected and mounted in acrylic. Micro-computerized tomography (μ -CT) was performed to assess bone to implant contact (BIC) and load analysis was performed using a Universal Test System. Three force applications were conducted until failure: pull-out (tensile), buccal push from the lingual (shear), distal push from the mesial (shear). The osteotomy sites were examined using light magnification and scanning electron microscopy (SEM).

Results: Pull-out, buccal and distal force failures occurred at differing levels. Post detachment sites showed complex patterns of bone failure, including trabecular and cortical fracture, as well as shearing at varying distances from the BIC. Interfacial shear strength was calculated at 14.4 MPa.

Conclusion: The osseointegrated RBIs were able to withstand simulations of the demanding axially, bucco-lingually and mesio-distally oriented biomechanical challenges of the posterior saddle, under conditions of reduced bone volume. These values exceeded equivalent force components of maximal masticatory loads in humans.

Acknowledgements: This research was assisted with funding kindly provided by the Melbourne Dental School, University of Melbourne, and the Australian Prosthodontic Society

Word Count: 7000 words

1 Introduction

Although short implant supported prosthodontic success for the resorbed posterior saddle has been reported as high (Rosentiel et al. 2006), caution has been expressed through a heavy emphasis placed on careful patient selection, underpinning diagnosis, and treatment planning to achieve this success. This problem is especially evident in the mandibular posterior saddle, where occlusal loads are high (Kan et al. 2014) and where after many years the ridge is resorbed. Furthermore, there is an increased proximity to the underlying inferior dental nerve, which if damaged, poses significant risk of facial numbness or paraesthesia.

The importance of implant design in addressing functional demands has been extensively discussed (Misch 1999; Cehreli et al. 2004). This research project poses a novel design of

dental implant, the Rectangular Block Implant (RBI). It is specifically designed to address the needs of patients with this clinical problem. It represents a new concept in implant design and force distribution (Gazelakis 2019).

This endeavor is not designed to replace the plethora of dental implant designs that currently exist. It is aimed at providing a specialized implant fixture for a particular clinical application, that is, the restoration of the resorbed alveolar ridge. The RBI presents a novel approach in that its longitudinal axis is along the mesial-distal length of the remaining ridge which is the very dimension in which nature preserves the maximal remaining bone volume, while its flat surfaces provide an even force distribution and maximizes surface area.

The aim of this article is to qualitatively analyze the biomechanical characteristics of the osseointegrated RBI in determining its maximal ability to withstand unfavorably applied loads, in bucco-lingual, mesio-distal shear directions and retentive tensile occlusal direction. Although this analysis is focused on linear maximal loads to failure, no biomechanical assessment can be complete without corresponding stress-strain analyses, and their relevance with respect to bone structure and physiology (Frost 1987). Such work has been conducted will be the subject of a further paper.

2 Materials and Methods

2.1 Implant design and manufacture

After designing and manufacturing the RBI (Ti-Grade IV) through CAD (CNC Lathe Turning, Phantom Engineering, South Australia), its grit blasted/acid etched surface topography was calibrated to industry norms. The external design was a rectangular body of 6mm length, 4mm bucco-lingual width and 5.25mm crestal-apical height. The external face had a series of macroscopic grooves. Figure 1 and Table 1 outline the design of RBI. The assembly coupling was a taper-integrated-screw-fit design (Bozkaya & Muftu 2003).

The coupling was an internal connection. This consisted of (proceeding crestal-apically):

- 1 A mesio-distally oriented finned anti-rotational geometry
- 2 A truncated conical engagement surface
- 3 The threaded elements (x 5).

For greater details, readers are referred to patents: Europe and the United Kingdom (16788970.8 – 1126); Australia (2016257149 B2).

2.2 Animal Surgery

The surgical protocol evaluation and clinical testing were achieved through placement of 12 RBIs into three mature greyhound dogs (two males, one female) in their posterior edentulous mandibles (2 per side). This animal model was chosen on the basis of its thin mandibular structure and underlying inferior alveolar nerve neurovascular bundle, closely simulating that of the human structure in the edentulous state (*see* Discussion). General anaesthesia was achieved with 15 mL Propofol via a cephalic vein catheter and maintained with intubated endotracheal machine-driven oxygen and 2% Isoflurane. The osteotomy sites were prepared with piezo-surgery tooling (Mectron Corporation, Italy) to produce a rectangular trough. A trial fit RBI was used to assist osteotomy trough construction to a set 0.5 mm smaller dimension in both mesial-distal length and bucco-lingual width than the intended block implants. The RBIs were press fitted with mallet and centre punch action and all implants were seated firmly into position without lateral wall surface exposure (Figure 2). Primary stability was achieved through the creation of a slightly undersized osteotomy site (0.5 mm in both the mesial-distal and bucco-lingual aspects) and the passive seating of the trial fit gauge to a level of approximately 80% into the osteotomy site. Primary stability was tested by hand grip of the attached stem. The latter was provided in varying lengths for 2 – 3 cm.

The flat faced base of the RBI (surface area of 24 mm²) facilitated high insertion mallet forces with implants being placed to within 1-2 mm from the superior border of the mandibular canal.

A two-stage surgery technique was adopted. Cover screws were engaged (finger pressure only), muco-periosteal flaps were repositioned (4 0 Vicryl, Johnson and Johnson, Australia) and implants were allowed 3 months to heal.

2.3 Osseo-integration

This was assessed clinically at second stage surgery exposure, at which time, the animals were sedated, and then euthanased through administration of 20 mL of sodium pentobarbitone (325 mg/mL), into the right cephalic vein.

Resonance frequency analysis (RFA) [Osstell, W & H Pty Ltd., Australia, Smart Peg #47] and torque tests (torque wrench: Nobel Biocare, Australia) applied through a cylindrical healing abutment, were performed. These results were compared with similar tests done on previous placements in a freshly killed dog mandible, to simulate the baseline non-integrated state. Successful clinical osseointegration was deemed to have been achieved if an implant produced Osstell readings over 80 from all directions (mesial, distal, lingual and buccal) as well as five torque test levels of over 35 Ncm.

After second stage clinical testing, the healing abutments were left in position. The mandibles were carefully dissected, de-fleshed and implant bone blocks produced, for micro-computerized tomography (μ -CT), using the SkyScan bench-top, μ -CT machine [1172 High Resolution, Bruker Corporation, Kontich Belgium] and scanning electron microscope (SEM) [Zeiss Gemini II Electron Microscope, CSIRO, Clayton Victoria]. Micro-CT utilized an Al-Cu (beam pre-hardening) filter with a beam hardening correction factor of 35%.

Micro-CT (a non-destructive method) was utilized for bone to implant contact (BIC) evaluation, while SEM was utilized post-force application, for evaluation of the implants and the osteotomy sites after failure. Micro-CT images were assessed by eye (less than x 5 magnification): - the threshold here for positive contact was at ≤ 0.2 mm. The greyscale (0-255) range was used to assess the presence or absence of bone, where the middle range (~ 85 -170) of whiteness was subjectively assessed as being indicative of bone tissue.

2.4 Loading Tests

All loading tests were performed using an Instron Universal Testing System Machine [Model 5544, Melbourne, Australia]. Three dissected RBI-bone blocks were used, each containing 2 osseointegrated RBIs: one mesial and one distal. The bone blocks were embedded in acrylic (Trad Cold Cure, GC Corporation Japan) which was trimmed to size and loaded onto the platform of the calibrated Instron Machine.

The biomechanical assessment of the osseointegrated bone-RBI complexes was tested through three directional force applications: pull-out tensile retention, buccal push shear mode from the lingual, and distal push shear mode from the mesial. The pull-out tensile tests were achieved through a chuck grip action onto a 4 mm diameter cylindrical healing

abutment torqued to 50 Ncm. Push shear mode tests were performed with titanium stems engaged in the RBIs with the purchase point of the push arm 1.0 mm from the face of the implant.

After calibrating the load cell with a precision 10 kg load, the machine was set to pull or push on the abutment cylinder at a slow, constant rate (0.05 mm/min). The pull-out tensile or push shear forces were measured electronically by the calibrated load cell, which recorded the peak force before failure. Forces were recorded to the nearest 0.1 N. Accuracy was deemed at ± 0.5 N for the 1000 N load cell. Post failure, fractured bone surfaces were analysed under light magnification (x10).

2.5 Animal Ethics

All procedures were performed under Animal Ethics approval (Ethics ID: 1112344.1: Animal Ethics Committee, University of Melbourne). The approval for this *in vivo* animal model and its selection was based on its ability to mimic the human resorbed alveolus after creation of edentulous posterior regions.

The animals were housed at the Animal Hospital Facility, School of Veterinary Science, University of Melbourne. All animal husbandry, pre-operative, operative and post-operative care was undertaken here by trained animal care staff and technicians. This included animal anxiety control, nutrition, exercise, hygiene and cleanliness. Animal anaesthesia and drug administration was performed by veterinary surgeons within this facility.

The animal experimentation protocol (including the research question, key design features, and analysis plan) was prepared prior to the commencement of this study, and submitted for approval (and retained) by the Animal Ethics Committee, at the University of Melbourne.

Upon approval, the conduct and reporting of the study were executed in accordance with the principles of Enhancing the Quality and Transparency Of health Research (EQUATOR), which are embodied by Percie du Sert et al. (2020) as applied to animal experimentation: Animal Research Reporting In Vivo Experiments (ARRIVE).

3 Results

3.1 Osseo-integration

Eleven of the 12 implant placements passed both RFA and torque test assessment of osseo-integration clinically (Tables 2, 3). Micro-CT showed extensive regions of trabecular contact as well as marrow spaces and regions of non-integration (Figure 3). Linear surface quantified bone to implant contact (BIC), had a mean percentage level of 46.9 ± 5.3 % of the total implant surface, as determined using μ -CT.

Applying a 50/50 random chance of passing any given clinical test ($\pi = 0.5$), an applied binomial distribution of obtaining 11/12 implants having passed both tests, yields a confidence interval (against a random outcome) of $p < 0.01$.

3.2 Pull-Out Tensile Tests

3.2.1 Pre and Post Integration Pull-Out Values Achieved

Two pre osseo-integration pull-out tensile tests performed on dead animals yielded detachment failure at 115.1 N and 116.9 N respectively. These served as a baseline comparison for post integration pull-out tensile tests and yielded an understanding of the degree of primary retention achieved upon initial placement.

Post integration, the RBI pull-out tests (x2) yielded 685.0 N and 712.9 N (Figure 4). Magnified evaluation of the pull-out site and the removed RBIs showed differing morphologies of trabecular bone shear.

3.2.2 Post Pull-Out Integrated RBI and Osteotomy Site Assessments

The overall osteotomy site upon pull-out, retained its original rectangular shape. It was evident that the pull-out produced three levels of detachment mainly at the vertical interface surfaces of the implant and bone. Firstly, implant-bone shear: - this detachment left titanium surfaces that were previously osseo-integrated, exposed and stripped of bony coverage. Secondly, trabecular bone shear: - this detachment left titanium surfaces still covered with osseo-integrated bone coverage. Thirdly, cortical shear: - this detachment only occurred on

the inter-implant crestal bone (Figures 5 & 6).

3.3 Bucco-Lingual Push Shear Tests

The bucco-lingual push shear test results yielded failures at 489.1 N and 500.2 N. Upon force application, the stem showed signs of plastic deformation, before failure of the implant-bone interface which coincided with failure of the entire buccal bony wall. Movements of the Instron push arm emanating from such fatigue and “settling” of the sample-system created deflections in the force-time plot (Figure 7) leading up-to the point of failure.

Unlike the positive force readings of the tensile (pull-out, Fig 4) actions, the above readings of (compressive) push actions, were negative in character. Implant sites showed cortical bone fracture on the buccal (compressive) side (Figure 8) and bone shearing and shredding on the lingual (tensile) side. Upon force application, the stem showed signs of deformation, before ultimate failure of the implant-bone interface.

3.4 Mesial-Distal Push Shear Tests

The distal push shear test results yielded failure at 800.9 N and 947.1 N. This latter value occurred due to titanium rod fracture, and not a complete implant displacement. Upon load application for both implants, the stem began to flex and distort at its minimal shaft (threaded) dimension. Fluctuations along the force-time plot up to the point of failure were experienced and closely observed as small settling movements in the mounted assembly and plastic deformation of the engaged stem. These did not reflect any movement of the implant in its bony position (Figure 9).

On load application, there was a distal tipping moment. The trabecular surface on the advancing front was evenly compacted against the block face, representing an even force distribution (stress minimization). The apical block corners also provided further resistance to

displacement by their impingement into the adjacent bone walls producing a counteractive resistance to the tipping (Figure 10).

4 Discussion

4.1 The Animal Model

The greyhound dog has emerged as a suitable model for implant studies (Kimmel & Jee 1982; Branemark 1983; Judge 2006; Weng et al. 2003; Kan et al. 2014), as post-extraction healing provides saddles *comparable* (but not identical) to those in humans. A similarity was the proximity of the mandibular canal to the regions of RBI placement (Figure 11).

4.2 Surgical Considerations

4.2.1 Osteotomy Preparation Requirements

Although the Mectron unit was utilized, it should be clarified any modality of ultrasonic instrumentation capable of producing linear cuts in bone to depths of approximately 5.5 mm could be used. To this effect, there is a large variety of ultrasonic tools and reciprocating saws in the current market that would suffice.

It is acknowledged that the time involvement in preparing a rectangular osteotomy is *prima facie* a challenging procedure. To this extent, two endeavours are pertinent to reduce the time and are incorporated into the forward design ready for human trials:

- 1 The use of individualized printed surgical guide to outline the osteotomy site.
- 2 The creation of bespoke rectangular piezo-surgical instrumentation which will facilitate both the mesial-distal dimensions of the trial fit gauge and its depth.

The typical scenario of the application of the RBI is where anterior teeth are present, and correspondingly, adequate anterior alveolar bone volumes are maintained. The posterior saddle is the primary aim for the RBI application. As such, the anticipated posterior minimal bone volumes will be governed by mesio-distal length, bucco-lingual width and apical-crestal height: - the width and height emerge as critical volumetric parameters. To this effect bucco-

lingually, it is anticipated that approximately 6 mm of crestal width is required. This may increase as the block proceeds apically, and does not take into consideration the osseous elements that form the base of the corpus inferior to the mandibular canal. At least 6.25 mm of height is required above the mandibular canal to the crest, such that at least 1 mm of clearance is achieved between the base of the RBI and the superior border of the canal. Although the anterior and basal elements of the mandible are at a distance away from the anticipated RBI's position, work by Judge (2006) as well as by Kan et al. (2014) have highlighted the ability of the mandible to act as a single functional unit where stresses are dissipated through the generation of strains throughout the entire body, notwithstanding that the load application is in the posterior region.

4.2.2 Localized Bone Considerations

The stability achieved at the time of placement is purely mechanical, and there is a reliance on stresses generated within the peri-implant bone through the deliberate mis-match between osteotomy site and implant dimensions. The form of the implant surface rather than the surface roughness itself has been highlighted as the critical bone interface stress determinant (Skalak & Zhao 2000). It is further acknowledged that the RBI surgical implantation would have induced some undefined degree of damage to the interfacial bone (Huja et al. 1999). The importance of these factors are their ramifications in compromising bone biomechanical properties (Lambers et al. 2013) and inducing localized adaptive bone remodelling, including increased resorption mediated porosity (Herman et al. 2010). The issue of stress/damage induced remodelling is further compounded in the dog animal model which at the chosen surgical exposure stage of 12 weeks, coincides with only one complete bone remodelling cycle (Roberts 1988). These remain unknown biomechanical variables and require further analyses.

4.3 Osseo-integration

4.3.1 Micro-CT

Limitations of desktop μ -CT systems for the investigation of the BIC around metal implants, are related to metal-induced artefacts. Bernhardt et al. (2012) have highlighted the "noise" and scatter generated from the inherent differential in the attenuation properties between titanium and bone, when using conventional μ -CT. Furthermore, Stoppie et al. (2005) have explained that the titanium causes a blurred border of 60 μ m along the whole implant surface:

- metal artefacts are due to a combination of beam hardening, scatter and nonlinear partial volume effects. This is in congruence with Liu et al. (2012) who found an exclusion zone of 48 μm from the implant surface.

The $\mu\text{-CT}$ images of BIC in this study were assessed by eye (less than x 5 magnification). This falls outside the sensitivity of the aforementioned issues. The threshold resolution at the current level of analysis for positive contact was at ≥ 0.2 mm. This was deemed sufficient in this study as the prime objective was a (non-destructive) method to visualize bone volume as well as contact, such that they could be correlated to clinical and (destructive) biomechanical results.

The subjective analysis in this study of bone within the middle third of the greyscale, is acknowledged. Further studies will utilize a systematically calibrated digitized method of selecting only those pixels in the middle third of the greyscale. A further allowance will also need to be made depending on the beam hardening range of the machine used. This will require several calibrated images of samples of known bone densities.

4.3.2 Resonance Frequency Analysis

It is conceded that the use of RFA to assess osseo-integrated implant stability has hitherto been limited to cylindrical implants, and there is no definitional standard that links this test to the exact external morphology of any implant design. The RFA reading of 80 ISQ was chosen firstly on the basis that this level has been embraced clinically as being reflective of high implant stability (Meredith et al. 1996; Meredith 1998). Secondly, the ISQ readings of the *ex vivo* placements were consistently below 80 (Table 1), despite having excellent primary stability: - ultimately, the conclusion of successful osseo-integration was based on the *relative* RFA difference between the *ex vivo* and *in vivo* (12 weeks post-operative) placements.

4.3.3 Reverse Torque Tests

It is acknowledged that the application of the clinical torque test to determine osseo-integration of the RBI involves a disparity in applying a torsional load to a non-cylindrical structure. Two factors are relevant to this issue.

Firstly, the application of a torsional load can induce localized stresses at the implant-bone interface, notwithstanding whatever shape the implant may be.

Secondly, it is acknowledged that the torsional test was applied as an accepted industry clinical tool, purely in making a comparison between implants of identical geometry. The disparity in geometry between a RBI and cylindrical implants highlight the benefits of rectangular geometry for torsional stability: - that is however, without a calibrated comparison to cylindrical implants.

4.4 Pull Out Tensile Test

4.4.1 The Axial Direction and Surface Area

The press-fit process appeared to have yielded a high degree of immobility, conducive to osseointegration, as evidenced by the post-integration pull-out tensile force readings, which approximated to 700 N. The pull-out force is axial. Hence, the longer the implant in the axial direction, the greater the resistance to pull-out. Although pull-out tests have been performed in the past (Baker et al. 1999; Chapman et al. 1996), the move away from the press fit implant design over the decades, has been reflected in the decline of these studies. Keeping this in mind, it is pertinent that past tests (Li et al. 1999; Kraut et al. 1998) able to produce pull-out results over 700 N, required cylindrical implant lengths of greater than 10 mm in axial length. The axial length, or corresponding depth of the RBIs, in this study was significantly less, at only 5.25 mm.

The surface area of the block was 129 mm² (excluding the crestal face). Ignoring groove morphology, this equated to that of a cylindrical implant, 4 mm in diameter and approximately 10.2 – 9.2 mm in length, depending on apical contours, and ignoring thread morphology. This equates to the same surface area available for integration as that of a medium length cylindrical implant as described by Hobkirk & Wiskott (2006). The total surface area of osseointegration is significant, in that although not necessarily aligned with the path of axial displacement, osseointegrated surfaces provide shear force resistance to axial displacement (Butz et al. 2011).

4.4.2 Interfacial Shear Strength

The tensile bond strength of the titanium-bone interface has been well documented (Aspenberg & Skripitz 1998; Edwards et al. 1997). Brunski et al. (1999) have outlined the calculation of interfacial shear strength of osseointegrated implants as the applied force divided by the total surface area multiplied by the percentage bone to implant contact. This

would imply a complete detachment between the implant and its bony integration, leaving a denuded implant surface.

From the results of the osseo-integration component of this project, a conservative overall bone to implant contact was estimated at 38%. With an overall surface area of 129 mm² and mean pull-out forces of 704.0 N, this equates to a mean interfacial shear bond strength of 14.4 MPa. This figure is approximately one order of magnitude higher than those reported by Brunski (1999) and significantly greater than those of others (Taylor et al. 1992, Steinemann et al. 1986).

4.4.3 The Block Shape and Trabecular Fracture

As a block, the implant has four surfaces parallel to the axial direction, four corners and cornered edges, which are axially oriented. While the four surface-planes offer axial resistance to shear pull-out displacement, the corners offer maximal interfacial surface resistance to displacement. The pull-out tests done on dental implants in the past have all been press-fit cylindrical structures. The conclusion is that the rectangular shape of the current structure offered greater retentive and resistive form.

Secondly, it was apparent that the mechanism of osseo-integrated implant displacement is not simply a matter of overcoming the bone-titanium interfacial bond. Evaluation of the pulled-out blocks and their corresponding osteotomy beds revealed different levels of bony detachment. There were areas of exposed titanium that represented osseous detachment at the implant-bone interface. There were however, other regions that represented more distant trabecular detachment that left both grooves filled with bone as well as regions of attached trabecular bone on the surface of the block. These regions of attachment corresponded with “gouged” areas of missing bone from the osteotomy wall, produced by trabecular shredding and fracture. It is postulated that the bone inter-locking action of the transverse surface grooves of the blocks established a heterogeneous macroscopic topography that underpinned the nature of bony detachment.

Cowin et al. (1987) noted that the tensile strength of fully mineralized trabecular (cancellous) bone is in the order of 100 to 150 MPa, and the interfacial (bone to new bone) shear strength of bone is 68 MPa. It follows that pull-out events necessitating greater and more distant level of trabecular bone fracture will require higher force levels. This will correspondingly increase where cortical elements are involved, where the tensile strength of bone can increase ten-fold. Wong et al. (1995), showed that for implant surfaces with different roughness but the same implant shape, site, and implantation time, there is a nearly linear relationship between the

“pushout load to failure” and surface roughness in microns: The highest shear strength in that study was approximately 7 MPa, for hydroxy-apatite surface coated implants with a surface roughness of 6 to 7 μm . It must be clarified that the pull-out and push tests of the literature described pertain to implant surfaces that had been indeed roughened to varying degrees, but were nonetheless classified by Bruski et al. (1999; 2000) as “smooth” with respect to macroscopic features. They opined that in the absence of macroscopic bone interlocking features, the predominant strength of the bone-implant interface is derived from the cement based osteoid, and will not exceed much more than the results achieved by Wong et al. (1995), and that although the tests pertain to interfacial shear forces, they still fall far short of the documented interstitial bony interfacial shear strength.

The ramification from the above is that the macroscopic bone interlocking of the block surfaces, corners and grooves, coupled with the presence of microscopic osseointegration, recruits the tensile strength of the trabecular elements and crestally, the cortical elements. The final result is a pull-out event that involves a continuum: - from pure interfacial shear, to trabecular tensile fracture close to the peaks of the grooves, and ultimately in some areas, to trabecular tensile fracture beyond the peaks of the grooves and even implicating the cortex. The apical (bottom) face of the RBI would also have contributed to the tensile pull-out strength. Given that this surface did not have any grooves, the detachment force contribution here would equate to the total osseointegrated area (BIC) multiplied by the estimated trabecular bone shear strength per unit area. The exact evaluation of this contribution remained outside the scope of the current study.

4.4.4 Pull-Out Tensile Force Tests and Axial Loads

Although being in opposite directions, both the pull-out force tested here and the theoretical vertical loads of function, are ultimately axial loads. Any new design of implant must be able to withstand the masticatory forces for which it is intended. Bruski (2003) clarified that the axial component of the biting force in adults, in the posterior segments, is in the range of 390-880 N and it has been suggested that the general features of mastication in patients with normal and implant restored dentitions are approximately the same (Carlsson & Haraldson 1985).

The pull-out tensile force of the osseointegrated RBIs in this study was within the numerical range of the maximal compressive axial biting force (Kan et al. 2014) and it has been clarified that the natural bony architecture of the mandible is designed to maximally distribute the peri-implant strains and stresses generated. This is a critical factor that

underpins the ability of the implant-bone environment to withstand the axial loads (Judge 2006). Indeed, the RBI was able to withstand the requisite natural (apically directed) level of axial loads applied in the most unfavourable (pull-out) tensile direction. The corollary of this reasoning is that the tensile strength of the implant-bone interface of the osseo-integrated rectangular block, is able to easily withstand the compressive axial loads of the posterior occlusion as most failure would occur under tensile stresses rather than compression.

4.5 Push Shear Tests

4.5.1 Buccal Direction Shear Test Analysis

Although in the natural complete dentition the predominance of occlusal load is axial, actions of the upper palatal (occlusal aspect) and lower buccal (occlusal aspect) cuspal inclined planes produce buccally oriented horizontal force components (Bates 1975). These will induce tensile stresses in the buccal (and lingual) bony elements (De Las Casas et al. 2007).

Assuming an inclined cuspal plane action of 30° [as per International Standards Organization (ISO) Standard 14801], the horizontally resolved vector of the component of force normal to the cuspal interface will exert a horizontal static load that in the case of the implant borne crown, will need to be buttressed by the tensile and compressive strengths of the implant bone interface and beyond this, the buccal cortico-cancellous bone.

In the case of the current buccal push shear tests, the values of “horizontal” failure occurred at 489.1N and 500.2 N.

These loads equated to at least $489.1(\tan 30^{\circ})^{-1}$ and $500.2(\tan 30^{\circ})^{-1}$: - that is, 847.2 N and 866.4 N respectively of axial force. Hence, these are the axial loads that are required to produce the correspondingly reached maximal horizontal buccal loads. It is pertinent to note that these axial loads are within the documented ranges of maximal occlusal loads (Brunski 2003).

The implication is that the buccal RBI-bone interface in the current model can withstand the buccally (and lingually) oriented “horizontal” components of physiological non-axial forces generated from cuspal inclined planes (De Las Casas et al. 2007).

The successful implant must be conducive to an interface which can withstand these tensile and compressive stresses. Although the buccal load was compressive in nature, the lingual BIC was necessarily tensile. The entire buccal cortico-cancellous wall underwent catastrophic failure, prior to any detectable buccal displacement of the implant. This is in congruence with

the rectangular block's flat faced even distribution of applied compressive loads and stress concentrations at the edges.

It is postulated that in the case of the current applied buccal forces, this unique even-faced force distribution acted to minimize stress concentrations, with the whole face acting as an advancing front. The outcome was a more efficient transfer of the applied loads to the adjacent cortico-cancellous architecture which served to reduce mechanical reliance on the relatively weaker implant bone interface (Brunski 2003).

Further studies focused on the differential aspects of tensile and compressive failure, and higher magnification microscopy (SEM) as well as finite element analysis (FEA) are needed to further clarify the bio-mechanical elements of the block implant detachment in the buccal-lingual dimension.

4.5.2 Distal Direction Shear Test Analysis

In the current tests, the RBI-bone interface was able to withstand horizontally oriented mesio-distal forces of 800.9 N and 947.1 N. Again, using the above reasoning of the ISO 14801 inclined cuspal plane action of 30° (now applied mesio-distally), the "horizontal" loads equated to 1387.1 and 1611.2 N of axial force respectively. These values are beyond the maximal axial biting forces reported in the literature (Brunski 1999; Judge 2006).

These "horizontal" mesial-distal push shear tests represented an exaggerated horizontal component of the axial load on posterior implants that in practice can result through:

- (i) the action of opposing cuspal mesio-distal inclined planes: this may result in either mesially or distally oriented horizontal vectors (these calculations are identical to those above).
- (ii) the action of the mandible as a class III lever system, with a posterior point of pivot (especially in the presence of parafunction: Brunski et al. 2000). This would result in mesially oriented horizontal vectors.
- (iii) any tensile forces and bending moments generated by the use of large, cantilevered bridge spans, where the support of the distally cantilevered prosthetic platform is derived from only anterior implants.

4.6 RBI Design Characteristics: Clinically Related Issues

4.6.1 The RBI as a Short Implant

The use of short implants has been presented as a viable clinical option in areas of low bone volume, and this option has hitherto been approached with caution. Although clinical analyses (Chen et al. 2020) have highlighted risk factors associated with the failure of short implants, recent reviews have also highlighted the success of splinted short implants (Carosi et al. 2021: ≤ 6 mm) and immediate loading of short implants (Kulkarni et al. 2021: 6mm). Although the success of these short conventional implants is acknowledged, the RBI is designed to present a short (5.25 mm) implant which has an osseointegrative surface area comparable to that of a conventional tapered form implant of medium length (4 mm diameter and 10 mm length). Furthermore, the flat surfaces of the of the block design act to evenly distribute the applied loads across the implant bone interface, reducing the concentration of the generated stresses. This is in contrast to cylindrical forms, where stresses are maximal at the normal tangential interface with respect to the load.

4.6.2 Crestal Design and Peri-Implant Tissues

The crestal surface was finished as a machine polish. This is in line with all the current implant designs which ultimately have a clear demarcation between the roughened surfaces deemed for osseointegration and those that are positioned at or above the crestal bone level. There has been much discussion concerning the design provisions for platform switch and the impact of this design feature on the preservation of peri-implant tissue health (Degidi et al. 2008).

Aligned with this principle the RBI crestal surface dimensions and internal connection have been designed to yield 0.6 mm of platform switch at each of the buccal and lingual extremities, and over 1 mm at each of the mesial and distal extremities. The role that this effect plays in crestal bone preservation and the establishment of peri-implant tissue health, will be examined in future clinical studies and remains outside the scope of this discussion.

4.7 Limitations

Finally, it is acknowledged that the results of this study must be interpreted with caution, as it is lacking statistical power. Further studies are needed, where larger samples of implant bone blocks are used to yield results in all three spatial directions, and where failure can be tested statistically as an end point under linear regression analyses. The utilization of strain gauges

(Judge 2006; Duyck et al. 2000) in these samples would also yield data for future FEA of the osseo-integrated RBI.

These limitations were underpinned by both financial and ethical approval constraints. These constraints impacted directly on the number of implants and animals used, and hence the lack of controls as well as the small sample size.

Furthermore, histological evaluations were also affected as they are end-point procedures which preclude on the same animal sample, biomechanical end-point testing.

It is further conceded that this study is animal based, and caution should be imposed when extrapolating implications of these results to the human situation.

Author Manuscript

5 Conclusion

Within the limitations of this study, it appeared that the osseointegrated RBI was able to withstand simulations of the demanding axially, bucco-lingually and mesio-distally oriented biomechanical challenges of the posterior saddle, under conditions of reduced bone volume. The RBI provides the anatomical advantages typical of a short cylindrical implant and the biomechanical advantages of a larger surface area, typical of longer cylindrical counterparts. This biomechanical advantage is further enhanced by the flat surfaces of the RBI design which provide unique patterns of facial force distribution, thereby minimizing stress concentrations. Further clinical studies with greater sample sizes and FEA modelling are needed to confirm this proof of concept study.

Declaration of Interests

The authors declare that they have no financial or other conflict of interests in the conduct and reporting of this study. All intellectual property ownership rights remain vested in the University of Melbourne, and not the authors themselves.

ORCID

Efthimios Gazelakis: <https://orcid.org/0000-0002-3346-9281>

Joseph E.A. Palamara: <https://orcid.org/0000-0003-1439-4509>

References

- Aspenberg, P. & Skripitz, R. (1998) Tensile Bonding Between Bone and Titanium. In: *Transcripts of the 44th Orthopaedic Research Society*, (March 16-19). New Orleans, LA: (ORS), p. 220.
- Baker, D., London, R.M. & O'Neal, R. (1999) Rate of pull-out strength gain of dual-etched titanium implants: a comparative study in rabbits. *International Journal of Oral Maxillofacial Implants*. **14**: 722-728.

Bates, J.F., Stafford, G.D. & Harrison, A. (1975) Masticatory function: A review of the literature. *Journal of Oral Rehabilitation*. **2**: 349-361.

Bernhardt, R., Kuhlisch, E., Schulz, M.C., Eckelt, U. & Stadlinger, B. (2012) Comparison of bone-implant contact and bone-implant volume between 2D-histological sections and 3D-SR μ -CT slices. *European Cells and Materials*. **23**: 237-247.

Bozkaya, D. & Muftu, S. (2003) Mechanics of the tapered interference fit in dental implants. *Journal of Biomechanics*. **36**: 1649-1658.

Branemark, P.I. (1983) Osseointegration and its experimental background. *Journal of Prosthetic Dentistry*. **50**: 399-410.

Brunski, J.B. (1999) In vivo response to biomechanical loading at the bone/dental-implant interface. *Advances in Dental Research*. **13**: 99-119.

Brunski, J.B., Puleo, D.A. & Nanci, A. (2000) Biomaterials and biomechanics of oral and maxillofacial implants: Current status and future developments. *International Journal of Oral and Maxillofacial Implants*. **15**: 15-46.

Brunski, J.B. (2003) Biomechanics. In: Worthington, H.V., Lang, B.R., Rubenstein, J.E. (eds). *Osseointegration in dentistry: An Introduction*. Quintessence Publishing Co., Chicago. 49-83.

Butz, F., Ogawa, T. & Nishimura, I. (2011) Interfacial shear strength of endosseous implants. *International Journal of Oral and Maxillofacial Implants*. **26**: 746-751.

Carlsson, G.E. & Haraldson, T. (1985) Functional Response. In: Branemark, P.I., Zarb, G.A., Albrektsson, T. (eds). *Tissue-Integrated Prostheses*. Quintessence Publishing Co., Chicago. 155-163.

Carosi, P., Lorenzi, C., Laureti, M., Ferrigno, N. & Arcuri, C. (2021) Short Dental Implants (≤ 6 mm) to Rehabilitate Severe Mandibular Atrophy: A Systematic Review. *International*

Journal of Oral and Maxillofacial Implants. **36**: 30-37.

Chen, L., Yang, T., Yang, G., Zhou, N., Dong H. & Mou Y. (2020) Retrospective clinical analysis of risk factors associated with failed short implants. *Clinical Implant Dentistry and Related Research.* **22**: 112-113.

Cehreli, M., Sahin, S. & Akca, K. (2004) Role of mechanical environment and implant design on bone tissue differentiation: current knowledge and future contexts. *Journal of Dentistry.* **32**: 123-132.

Chapman, J.R., Harrington, R.M., Lee, K.M., Anderson, P.A., Tencer, A.F. & Kowalski, D. (1996) Factors affecting the pull-out strength of cancellous bone screws. *Journal of Biomechanical Engineering.* **118**: 391-398.

Cowin, S.C., Van Buskirk, W.C. & Ashman, R.B. (1987) Properties of Bone. In: Skalak, R. & Chien S. (eds). *Handbook of Bioengineering.* McGraw-Hill, New York. 2.1–2.27.

De Las Casas, E.B., de Almeida A.F., Cimini Jnr, C.A., Gomes, P.V, Cornachia, T.P.M. & Saffar, J.M.E. (2007) Determination of tangential and normal components of oral forces. *Journal of Applied Oral Science.* **15**: 70-76.

Degidi M., Iezzi G., Scarano A. & Prattelli A. Immediately loaded titanium implant with a tissue-stabilizing/maintaining design ('beyond platform switch') retrieved from man after 4 weeks: A histological and histomorphometrical evaluation. A case report. *Clinical Oral Implants Research.* 2008 **19**: 276-282.

Duyck, J., Van Oosterwyck, H., De Cooman, M., Puers, R., Vander Sloten, J. & Naert, I. (2000) Three-dimensional force measurements on oral implants: A methodological study. *Journal of Oral Rehabilitation.* **27**: 744-753.

Edwards, J.T., Brunski, J.B. & Higuchi, K.W. (1997) Mechanical and morphologic investigation of the tensile strength of a bone hydroxyapatite interface. *Journal of Biomedical Material Research.* **36**: 454-468.

EQUATOR. Equator Network. Enhancing the QUALity and Transparency Of Health Research. www.equator-network.org

Frost, H.M. Bone “mass” and the “mechanostat”: A proposal. *Anatomical Record*. (1987) **219**: 1-9.

Gazelakis, E. (2019) *The Rectangular Block Implant: A novel implant design for the posterior atrophic ridge*. PhD Thesis, University of Melbourne.

Herman, B.C., Cardoso, L., Majeska, R.J., Jepsen, K.J. & Schaffler, M.B. (2010) Activation of bone remodeling after fatigue: differential response to linear microcracks and diffuse damage. *Bone* **47**: 766-772.

Huja, S.S., Katona, T.R., Burr, D.B., Garetto, L.P. & Roberts, W.E. (1999) Microdamage adjacent to endosseous implants. **25**: 217-222.

Hobkirk, J.A. & Wiskott, H.W. (2006) Biomechanical aspects of oral implants. Consensus report of working group 1. *Clinical Oral Implants Research*. **17**(Supplement 2): S52-S54.

Judge, R.B. (2006) *An In Vitro and In Vivo Investigation into Masticatory Bone. Strain Using a Dog Model*. PhD Thesis, University of Melbourne.

Kan, J.P., Judge, R.B. & Palamara, J.E. (2014) In vitro bone strain analysis of implant following occlusal overload. *Clinical Oral Implants Research*. **25**: 73-82.

Kimmel, D.B. & Jee, W.S. (1982) A quantitative histologic study of bone turnover in young adult beagles. *The Anatomical Record*. **203**: 31-45.

Kraut, R.A., Dootson, J. & McCullen, A. (1991) Biomechanical analysis of osseointegration of IMZ implants in goat mandibles and maxillae. *International Journal of Oral and Maxillofacial Implants*. **6**: 187-194.

Kulkarni, V., Uttamani, J.R., Asar, N.V., Nares, S. & Tozum, T. (2021) Evidence-Based

Clinical Outcomes of Immediate and Early Loading of Short Endosseous Dental Implants: A Meta-analysis. *International Journal of Oral and Maxillofacial Implants*. **36**: 59-67.

Lambers, F. M., Bouman, A.R., Rimnac, C.M. & Hernandez C.J. (2013) Microdamage caused by fatigue loading in human cancellous bone: relationship to reductions in bone biomechanical performance. *PLoS One*. **8**: e83662.

Li, DH., Liu, BL., Zou, J.C. & Xu, K.W. (1999) Improvement of osseo-integration of titanium dental implants by a modified sandblasting surface treatment: An in vivo interfacial biomechanics study. *Implant Dentistry*. **8**: 289-294.

Liu, S., Broucek, J., Viridi, A.S. & Sumner, D.R. (2012) Limitations of using micro-computed tomography to predict bone-implant contact and mechanical fixation. *Journal of Microscopy*. **45**: 34-42.

Meredith, N., Alleyne, D. & Cawley, P. (1996) Quantitative determination of the stability of the implant-tissue interface using resonance frequency analysis. *Clinical Oral Implants Research*. **7**: 261-267.

Meredith, N. (1998) Assessment of implant stability as a prognostic determinant. *International Journal of Prosthodontics*. **11**: 491-501.

Misch, C.E. (1999) *Contemporary Implant Dentistry*. 2nd ed., Mosby Publishing Co., St. Louis.

Percie du Sert, N., Ahluwalia, A., Alam, S., Avey M.T., Baker, M., Browne W.J., et al. (2020) Reporting animal research: Explanation and elaboration for the ARRIVE guidelines 2.0. *PLoS Biol* 18(7): e3000411.

Roberts, W.E. (1988) Bone tissue interface. *Journal of Dental Education*. **52**: 804-809.

Rosentiel, S.F., Land, M.F. & Fujimoto, J. (2006) *Contemporary Fixed Prosthodontics*. 4th ed., Mosby Publishing Co., St. Louis.

Skalak, R. & Zhao, Y. (2000) Similarity of stress distribution in bone for various implant

surface roughness heights of similar form. *Clinical Implant Dentistry and Related Research*. **2**: 225 – 230.

Steinemann, S.G., Eulenberger, J., Maeusli, P.A. & Schroeder, A. (1986) Adhesion of bone to titanium. In: Christel, P., Meunier, A., Lee, A.J.C. (eds). *Biological and Biomechanical Performance of Biomaterials*. Elsevier Science Publishing, Amsterdam. 409-414.

Stoppie, N., Van Der Waerden, J.P., Jansen, J.A., Duyck, J., Wevers, M. & Naert, I.E. (2005) Validation of microfocus computed tomography in the evaluation of bone implant specimens. *Clinical Implant Dentistry and Related Research*. **7**: 87-94.

Taylor, J.L., Brunski, J.B., Hoshaw, S.J., Cochran, G.V. & Higuchi, K.W. (1992) Interfacial bond strengths of Ti-6Al-4V and hydroxyapatite-coated Ti-6Al-4V implants in cortical bone. In: Laney, W.R. & Tolman, D.E. (eds). *Tissue Integration in Oral, Orthopaedic and Maxillofacial Reconstruction*. Quintessence Publishing Co., Chicago. 125-132.

Weng, A., Hoffmeyer, M., Hurzeler, M.B. & Richter, E.J. (2003) Osseotite versus machined surface in poor bone quality: A study in dogs. *Clinical Oral Implants Research*. **14**: 703-708.

Wong, M., Eulenberger, J., Schenk, R. & Hunziker, E. (1995) Effect of surface topology on the osseo-integration of implant materials in trabecular bone. *Journal of Biomedical Materials Research*. **29**: 1567–1576.

Crestal Surface

Crestal surface finish	Machine (polish)
Crestal surface features:	Purchase points, anti-rotational opening
Purchase points: diameter and depth	0.3 mm 0.15 mm

Anti-rotational Geometry

Design	Mesial and distal fins either side of central shaft
Depth	0.8 mm
Length (mesio-distal)	4.4 mm

Engagement Geometry

Design	Truncated Cone
Depth	1.45mm (from base of anti-rotational geometry)
Crestal diameter	2.8 mm
Apical diameter	2.0 mm (positive stop)
Divergence angle (degrees)	7.85

Threaded elements

Thread type	M2 x 0.4
Total number of threads	5
Total length of threaded shaft	2.5 mm (plus lead for milling and tapping)
Clearance between seated screw and block floor	0.8 mm
Abutment screw	M2 x 0.4 (no lead)

External Features

Wall -wall curvature radius	0.5mm
Wall grooves thickness	can be variable: - 0.6 mm approximately
Wall grooves height off block wall	0.2 mm
Wall-base curvature radius	0.5 mm
Thickness of block floor	0.55 mm
Base form	flat (non-grooved)

Table 1. RBI Further Design Parameters: Tolerance 10 µm.

Trial Run	Osstell ISQ Reading		
	1	2	3
Position and Orientation of Probe			
Buccal, Bucco-Lingual	78	78	78
Lingual, Bucco-Lingual	78	78	78
Mesial, Mesio-Distal	78	78	78
Distal, Mesio-Distal	78	78	78

Table 2. Ex vivo RFA trial runs. ISQ readings immediately after placement.

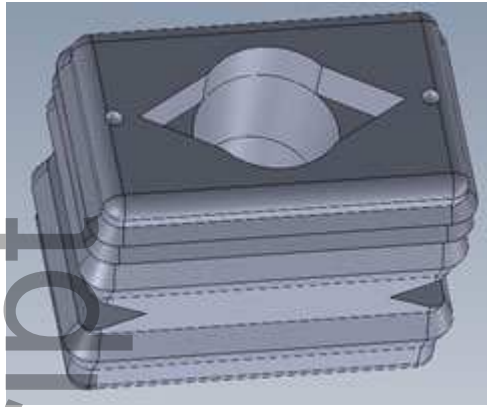
Author Manuscript

	IMPLANT	Osstell ISQ reading		IMPLANT	Osstell ISQ reading	
Left Side Animal 1	Distal	Buccal aspect	90	Mesial	Buccal aspect	87
		Lingual aspect	90		Lingual aspect	88
		Mesial aspect	90		Mesial aspect	87
		Distal aspect	90		Distal aspect	87
		35 Ncm torque test	Pass		35 Ncm torque test	Pass
Right Side Animal 1	Distal	Buccal aspect	85	Mesial	Buccal aspect	87
		Lingual aspect	85		Lingual aspect	87
		Mesial aspect	85		Mesial aspect	87
		Distal aspect	85		Distal aspect	87
		35 Ncm torque test	Pass		35 Ncm torque test	Pass
Left Side Animal 2	Distal	Buccal aspect	70	Mesial	Buccal aspect	81
		Lingual aspect	70		Lingual aspect	81
		Mesial aspect	59		Mesial aspect	81
		Distal aspect	59		Distal aspect	81
		35 Ncm torque test	Fail		35 Ncm torque test	Pass
Right Side Animal 2	Distal	Buccal aspect	88	Mesial	Buccal aspect	90
		Lingual aspect	88		Lingual aspect	89
		Mesial aspect	88		Mesial aspect	89
		Distal aspect	88		Distal aspect	89
		35 Ncm torque test	Pass		35 Ncm torque test	Pass
Left Side Animal 3	Distal	Buccal aspect	84	Mesial	Buccal aspect	80
		Lingual aspect	84		Lingual aspect	80
		Mesial aspect	84		Mesial aspect	80
		Distal aspect	84		Distal aspect	80
		35 Ncm torque test	Pass		35 Ncm torque test	Pass
Right Side Animal3	Distal	Buccal aspect	84	Mesial	Buccal aspect	85
		Lingual aspect	84		Lingual aspect	85
		Mesial aspect	84		Mesial aspect	82

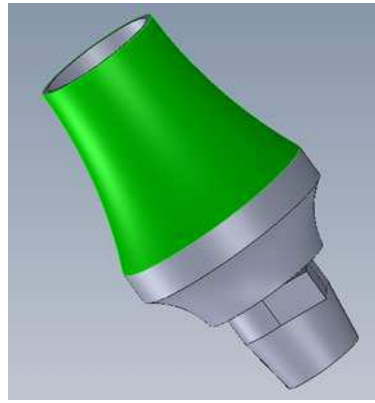
	Distal aspect	84		Distal aspect	82
	35 Ncm torque test	Pass		35 Ncm torque test	Pass

Table 3: Osseo-integration test summary: RFA readings and pass/fail torque test x 5. The relative change (over 80) of ISQ readings between ex vivo and in vivo (12 weeks post-operative) placements was taken as indicative of osseo-integration.

Author Manuscript



A Rectangular Block Implant



B Prosthetic Abutment

Figure 1: CAD (Solidworks Pty Ltd, USA). generated images of the RBI showing its series of macroscopic grooves (A) and its prosthetic abutment (B).



A.



B.



C.

Figure 2 (A, B, C): Surgical Placement Examples. A. The Rectangular Osteotomy Sites. B. Introduction of the RBI to the Osteotomy Site. C. Seated Implants.

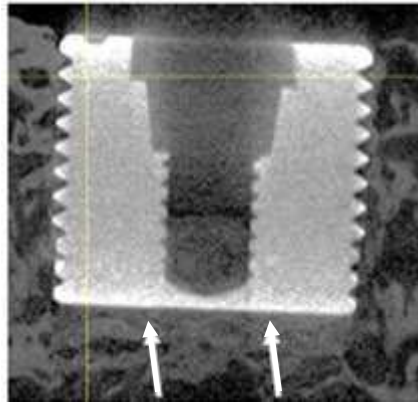


Figure 3: Micro-CT: Sagittal Slice. The mesial-distal and apical regions showed areas of implant-bony attachment as well as trabecular spaces. The apical bone showed particularly greater compaction near the implant surface (white arrows).

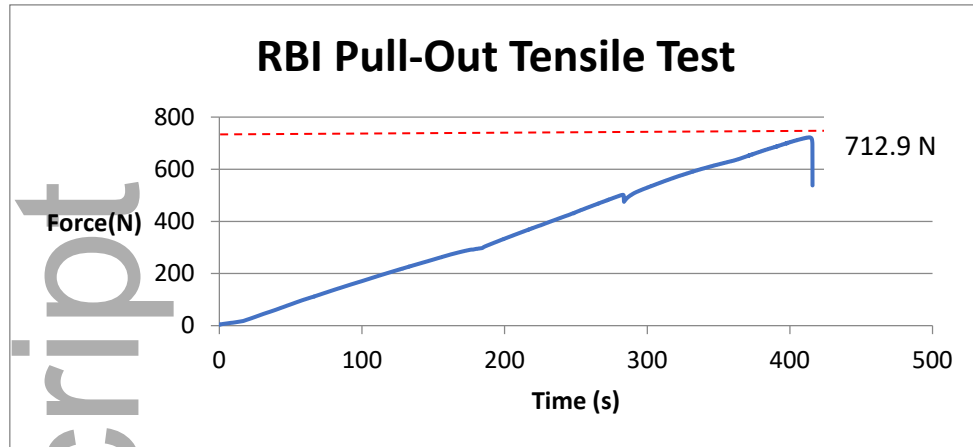


Figure 4: Shows a typical plot of the tensile pull-out post-integration.

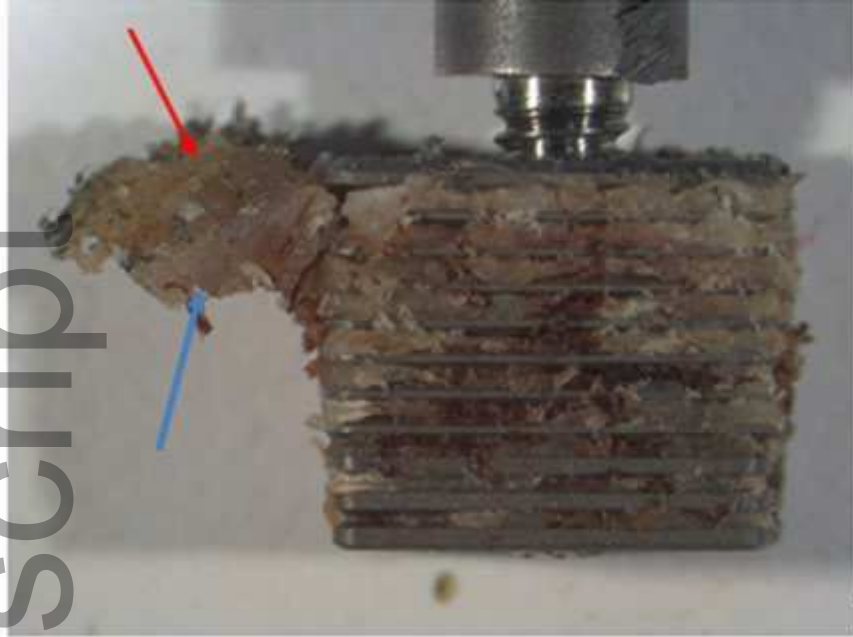


Figure 5: RBL post-integrated pull-out. The crestal cortical (red arrow) fragment also involved underlying trabeculae (blue arrow) which in turn implied stress fracture of the bone block inter-proximally.

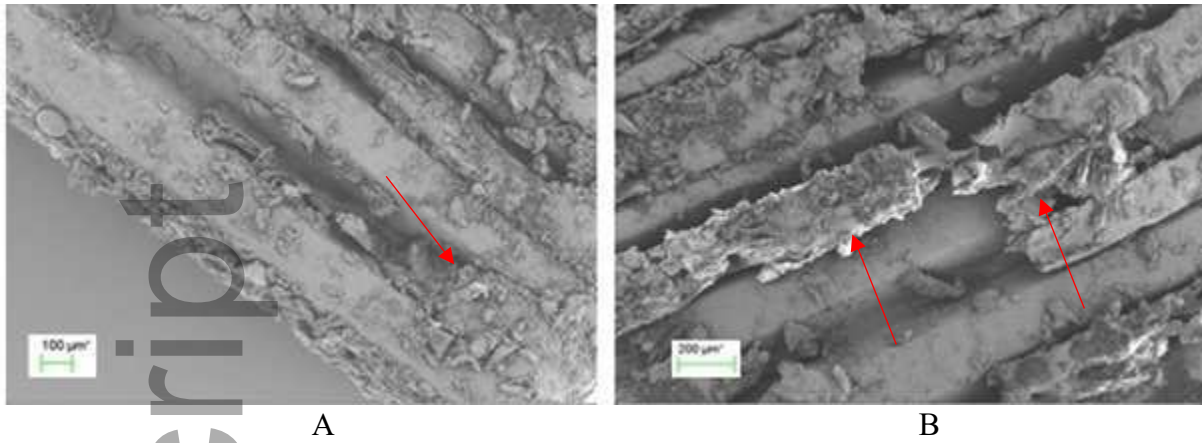


Figure 6 (A, B): (SEM original magnification, x 50) This shows evidence of trabecular shear, with the implant surface still coated with bony attachment (red arrows). This pattern of shear typically left bone at the depths of the grooves, and highly irregular trabecular morphologies.

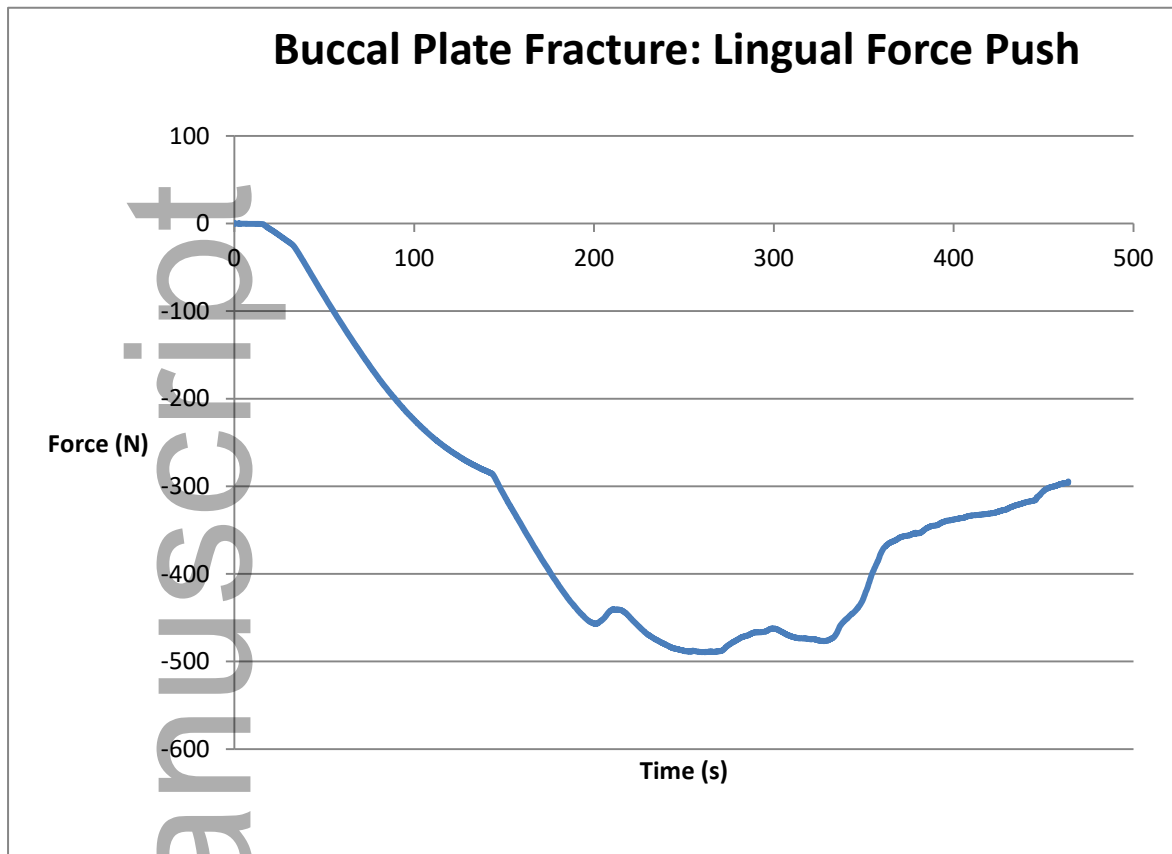


Figure 7: Shows a buccal push (shear force) test. Implant failure (489.1 N) coincided with complete buccal wall failure. Small fluctuations can be seen leading up to this point, as the buccal bony wall flexed under compression.

489.1 N

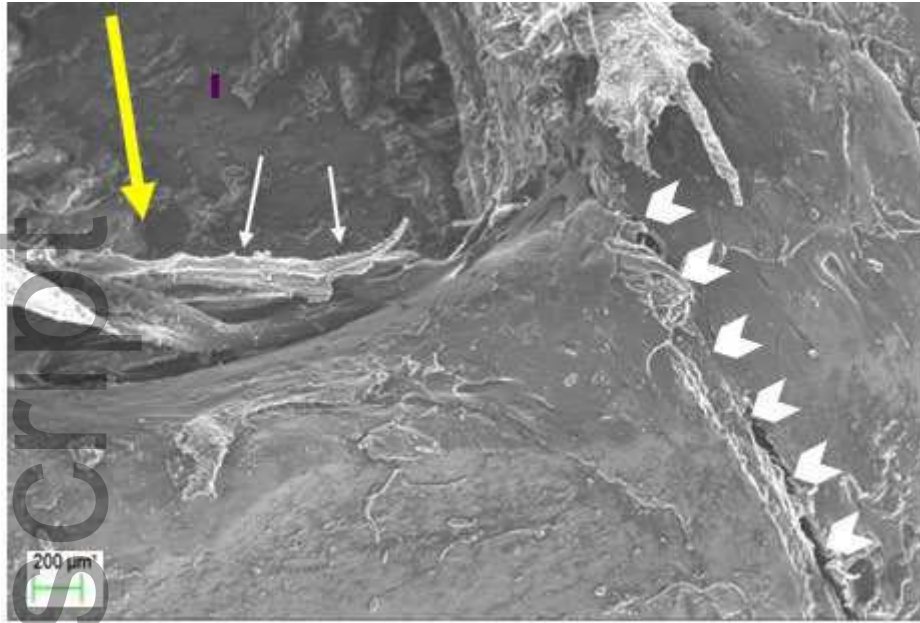


Figure 8: (SEM original magnification, x 30) This shows the buccal fracture line (white arrow heads) and bone shreds from the lingual aspect (white arrows). The shreds were buccally oriented. The force direction is shown (yellow arrow): lingual to buccal.

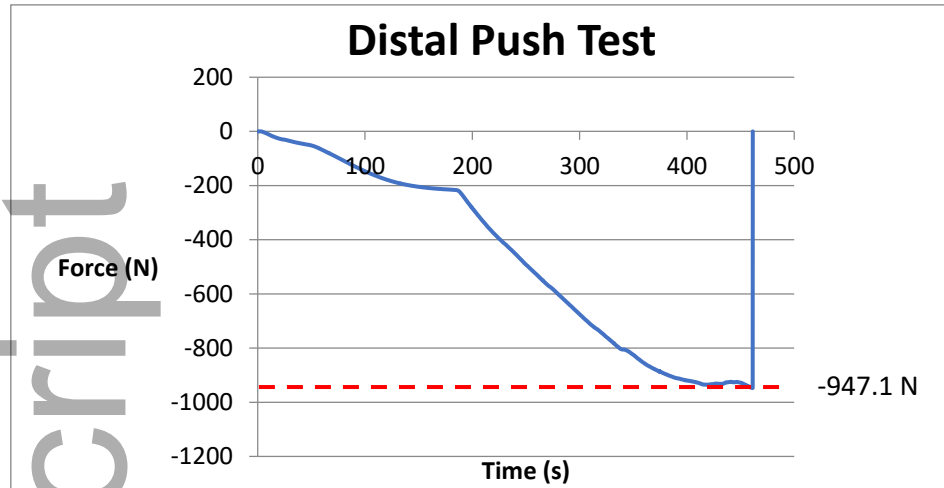


Figure 9: Force-Time plot shows non-linear load fluctuations up to the point of stem failure.

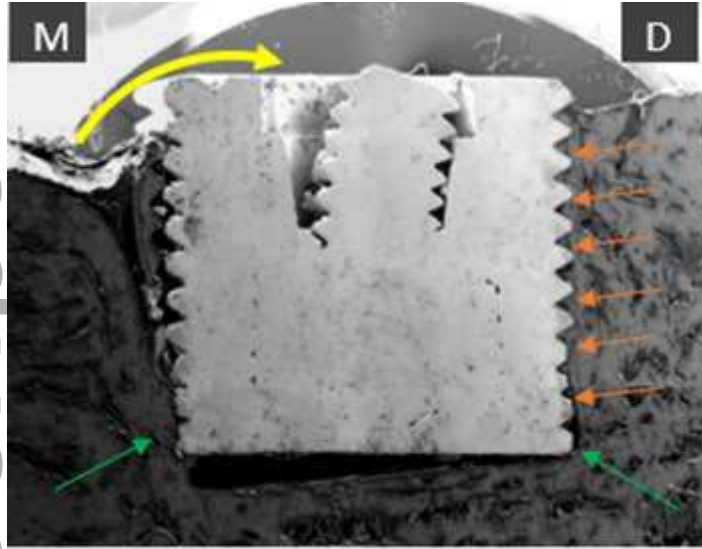


Figure 10: Mesial (M) – Distal (D) cut section. (SEM original magnification, x 10) This shows that upon the M force push, the entire surface of the advancing front pushed firmly against the D bony surface, due to the resultant moment (yellow arrow) experienced by the block. On D, the entire face appeared to be compressed against the bone (orange arrows), while the “crestal” aspect of the M surface had detached. The result was a fixed structure that had locked into place by the apical corners (green arrows).

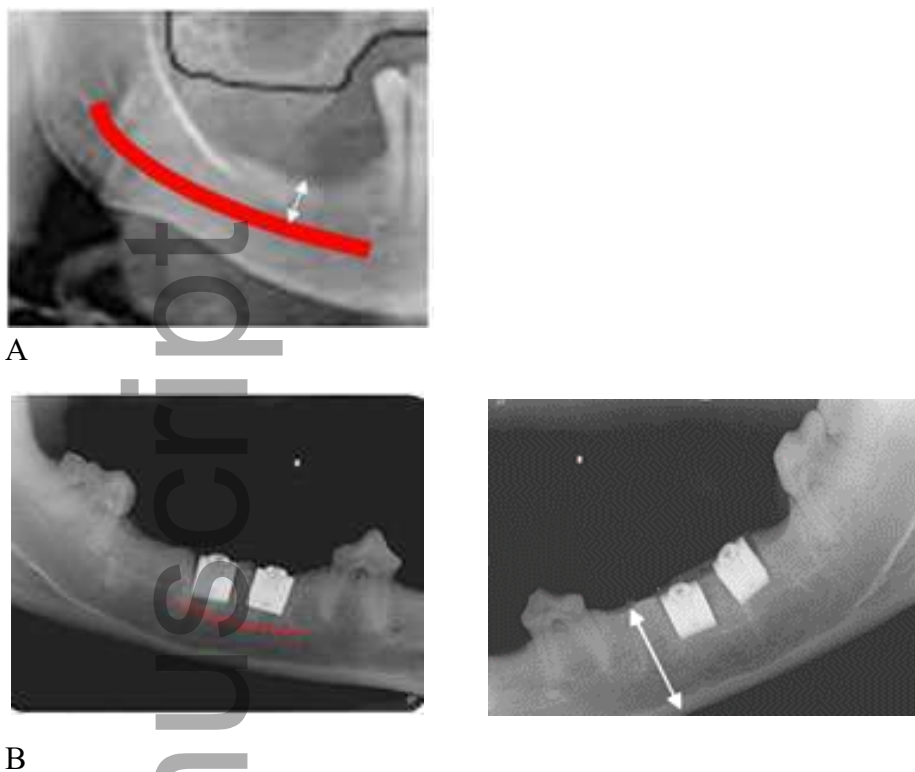


Figure 11 (A, B): Comparison between the greyhound edentulous saddle and that of the human.

A. Panoramic view of the human resorbed posterior alveolus. The white arrow represents in this patient an alveolar crestal height of approximately 6 mm above the superior border of the mandibular canal (red). Note the significant dimension of the corpus beneath the canal.

B. Panoramic reconstruction of the greyhound saddles (left and right) after implant placements allows some perspective of the anatomical dimensions of the greyhound edentulous posterior saddle, where the approximate height of the entire corpus is approximately 13 mm (white arrow) and the superior border of the mandibular canal (left side) is outlined (red).